analytical chemistry

pubs.acs.org/ac Article

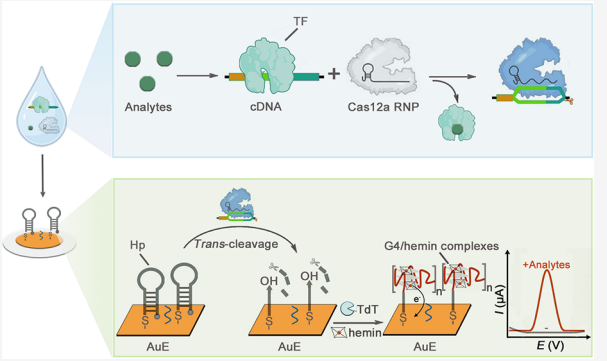
Label-Free Electrochemical CRISPR Platform Gated by Allosteric Transcription Factors for Ultrasensitive Small-Molecule Detection

Liang Zhu, Lejun Liao, Yan Huang,* Zhou Nie, and Chunyang Lei*

Cite This: https://doi.org/10.1021/acs.analchem.6c02971 Read Online

ACCESS | Metrics & More | Article Recommendations | Supporting Information

ABSTRACT: The highly sensitive analysis of small-molecule targets holds profound significance across diverse fields, ranging from clinical diagnosis and environmental monitoring to food safety. Herein, we developed a label-free electrochemical CRISPR platform gated by allosteric transcription factors (aTFs) for the ultrasensitive detection of various small molecules. In this system, the specific binding of target analytes to their cognate aTFs induces the release of programmable DNA adaptors, which subsequently trigger Cas12a to *trans*-cleave DNA probes anchored to the electrode surface. Consequently, the truncated DNA probes serve as initiators to form electroactive G-quadruplex/hemin complexes *in situ* via terminal deoxynucleotidyl transferase (TdT)-mediated elongation, generating a robust electrochemical response signal. Using TetR as a model aTF, this integrated electrochemical CRISPR biosensor achieved tetracycline detection with picomolar sensitivity. Furthermore, the versatility of this platform was demonstrated by extending its application to *p*-hydroxybenzoic acid and copper ions through the simple substitution of the aTF modules. The practical utility of the assay was further demonstrated by the robust detection of tetracycline in complex matrices such as milk. Ultimately, this study not only provides a novel strategy for constructing universal, label-free electrochemical CRISPR platforms but also paves the way for the sensitive detection of low-abundance non-nucleic acid targets.



Downloaded via SHENZHEN UNIV on July 6, 2026 at 02:07:08 (UTC).
See https://pubs.acs.org/sharingguidelines for options on how to legitimately share published articles.

INTRODUCTION

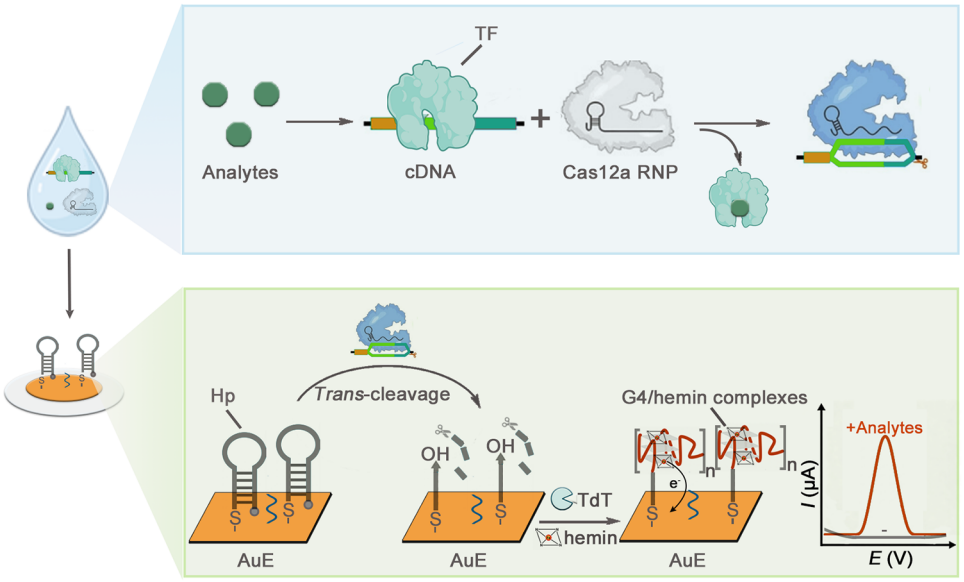
The highly sensitive and quantitative analysis of small-molecule targets is of paramount importance across diverse sectors, ranging from clinical diagnostics and environmental monitoring to food safety, where trace-level contaminants can pose significant public health risks.[1,2] Consequently, developing analytical methods that effectively combine high sensitivity with robust versatility remains a formidable challenge in the biosensing field. Recently, CRISPR/Cas12a-based systems have garnered immense interest in nucleic acid analysis, owing to their exceptional signal amplification capability triggered by target sequence-induced robust *trans*-cleavage activity.[3−7] Nevertheless, their intrinsic dependency on programmable nucleic acid sequences hinders their direct application to small-molecule analytes. To circumvent this limitation, researchers have integrated prokaryotic allosteric transcription factors (aTFs) as sensing modules into CRISPR detection frameworks.[8−10] This strategy leverages the highly specific conformational response of aTFs to target ligands to modulate the activation state of Cas12a.[8] Therefore, this approach effectively bridges the gap between CRISPR and small-molecule recognition, enabling the sensitive detection of various small molecules.

However, translating this versatile biological recognition into an accessible and sensitive readout remains a critical bottleneck for practical deployment. Current CRISPR-based biosensing systems primarily rely on fluorescent and colorimetric readouts.[11] Nevertheless, both optical modalities face practical constraints: Fluorescence methods offer good sensitivity but require sophisticated instrumentation for signal detection.[12,13] Conversely, colorimetric assays, such as lateral flow strips, provide excellent portability and simplicity but suffer from inherently low sensitivity, making it difficult to satisfy the requirements for the precise quantification of trace targets.[14−17] In contrast, owing to its ultrahigh sensitivity, rapid response, low cost, and ease of instrument miniaturization, electrochemical detection is regarded as an ideal candidate for the precise quantification of low-abundance targets.[18−20] Despite these advantages, constructing high-performance electrochemical CRISPR biosensors remains challenging. Specifically, current strategies face two primary limitations. First, they typically necessitate the covalent coupling of redox labels to DNA probes,[21−23] which complicates the sensor fabrication process. Second, the Cas12a-mediated *trans*-

Received: April 30, 2026
Revised: June 26, 2026
Accepted: June 29, 2026

© XXXX American Chemical Society

Scheme 1. Schematic Illustration of the Label-Free Electrochemical CRISPR Platform Gated by Allosteric Transcription Factors for Ultrasensitive Small-Molecule Detection



cleavage of immobilized DNA probes usually results in a "turn-off" signal mode.[24] Furthermore, in trace analysis, the "turn-off" mode often yields a poor signal-to-noise ratio due to high initial background signals.[24] As an initial step toward addressing these issues, our group recently developed an electrochemical interface for the label-free reporting of Cas12a *trans*-cleavage signals using hemin aptamers.[7] While this design successfully achieved label-free CRISPR detection, its signal transduction still followed a typical "turn-off" pattern. Therefore, engineering an electrochemical interface that simultaneously features a label-free architecture and "turn-on" signal amplification is vital for enhancing the reliability and practical utility of electrochemical CRISPR biosensors for small-molecule detection.

To address these challenges, we herein report a label-free electrochemical CRISPR platform gated by aTFs for the ultrasensitive detection of various small molecules. By coupling terminal deoxynucleotidyl transferase (TdT) amplification with the *in situ* generation of G-quadruplex/hemin complexes, this design effectively translates the CRISPR *trans*-cleavage event into an amplified, label-free, and "turn-on" electrochemical readout. In this framework (Scheme 1), target binding induces the dissociation of the aTFs from the programmable DNA adaptors; the unoccupied DNA adaptors subsequently activate the Cas12a ribonucleoprotein (RNP) to trans-cleave the hairpin DNA (Hp) probes immobilized on the electrode surface. Importantly, the intact hairpin structure initially contains a blocked 3′-end; however, Cas12a-mediated cleavage removes this block, leading to the exposure of an accessible 3′−OH terminus on each immobilized Hp probe. This critical structural switch allows TdT to catalyze the *in situ* synthesis of long G-rich single-stranded DNA sequences using a well-designed dNTP mixture. These G-rich sequences subsequently fold into G-quadruplex (G4) structures and bind hemin to form electroactive G4/hemin complexes, resulting in robust "turn-on" electrochemical signals. The versatility of this design was successfully demonstrated by the sensitive detection of tetracycline, *p*-hydroxybenzoic acid, and Cu^{2+} using their corresponding aTFs. The practical utility of the assay was further demonstrated by the robust detection of tetracycline in complex matrices such as milk. In summary, this study presents a label-free electrochemical CRISPR biosensing platform for the "turn-on" detection of small molecules, offering a new paradigm to expand the utility of CRISPR/Cas systems in biosensing.

EXPERIMENTAL SECTION

Chemicals and Reagents

Terminal deoxynucleotidyl transferase (TdT) was purchased from Thermo Fisher Scientific. TMB One Solution was obtained from Yisheng Bio. Isopropyl-*β*-D-thiogalactoside (IPTG), imidazole, kanamycin, dithiothreitol (DTT), and glycerol were supplied by Aladdin. Heparin sodium, Tris−HCl, deoxynucleotide triphosphates (dNTPs), and hemin were purchased from Sangon Biotech. All HPLC-purified RNA and DNA oligonucleotides (sequences listed in Tables S1 and S2) were synthesized by General Biology or Sangon Biotech. Oligonucleotide stock solutions (100 *μ*M) were prepared using DEPC-treated water and stored at −20 °C. All other chemicals were of analytical grade, and aqueous solutions were prepared with 18.2 MΩ·cm ultrapure water.

Protein Expression and Purification

The LbCas12a, TetR, HosA, and CsoR proteins were expressed and purified following established protocols.[8] The pET28a(+)-LbCas12a plasmid was provided by GenScript. *Escherichia coli* Rosetta (DE3) cells harboring the expression vectors were induced with 0.2 mM IPTG. Specifically, LbCas12a was expressed at 16 °C for 16 h. His-tagged LbCas12a was purified via Ni^{2+}-NTA affinity chromatography, washed with wash buffer (50 mM Tris−HCl, 1.5 M NaCl, 30 mM imidazole, pH 8.0), and eluted with elution buffer (50 mM Tris−HCl, 1.5 M NaCl, 600 mM imidazole, pH 8.0). The purified protein was dialyzed into storage buffer (50 mM Tris−HCl, 150 mM NaCl, 2 mM DTT, 10% glycerol, pH 8.0). Similar purification procedures were applied to TetR, HosA, and CsoR following expression under specific conditions: TetR (at 30 °C and 160 rpm for 16 h), HosA (at 20 °C and 160 rpm for 16 h), and CsoR (at 30 °C and 200 rpm for 5 h). Protein purity was verified by 12.5% SDS-PAGE at 110 V for 2 h and imaged using an Azure 300Q system.

Fabrication of the Electrochemical Biosensor

Gold electrodes (AuEs) were pretreated with piranha solution and polished with alumina slurries (1.0, 0.3, and 0.05 *μ*m) to a mirror

https://doi.org/10.1021/acs.analchem.6c02971
Anal. Chem. XXXX, XXX, XXX−XXX

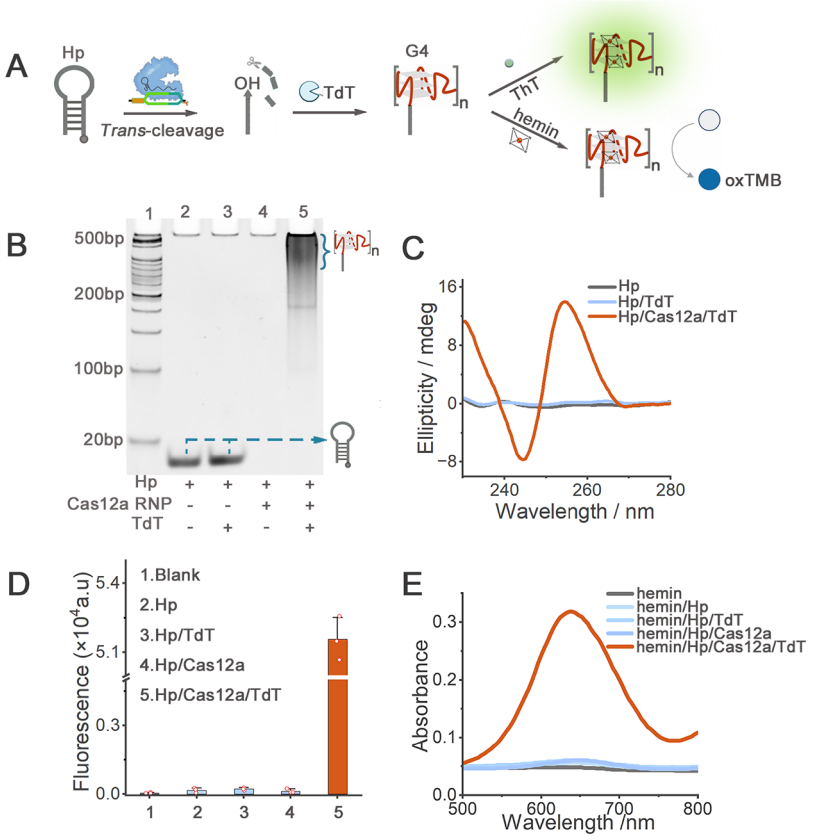


Figure 1. Verification of G4 formation via TdT elongation mediated by Cas12a *trans*-cleavage. (A) Schematic illustration of the Cas12a *trans*-cleavage-triggered TdT extension and subsequent formation of G4/hemin complexes through colorimetric and fluorescence verification. (B) Native PAGE (12.5%) analysis of the reaction products. Lane 1, 500 bp DNA ladder; lane 2, Hp; lane 3, Hp with TdT; lane 4, Hp with activated Cas12a RNP; and lane 5, Hp with activated Cas12a RNP and TdT. (C) CD spectra of Hp before and after treatment with Cas12a RNP and TdT in the presence of 50 mM K^+. (D) Fluorescence intensity of the system under different reaction conditions. (E) Absorption spectra of the TMB-H_2O_2 system catalyzed by the generated G4/hemin complexes. Data are presented as mean values with standard deviations (SD) derived from three independent experiments.

finish. The electrodes were electrochemically cleaned in 0.5 M H_2SO_4 by cyclic scanning from −0.3 to 1.5 V until a stable voltammogram was obtained. For probe immobilization, 5 μL of DNA hairpin (Hp, 2 μM) in HEPES buffer (10 mM, pH 7.0, containing 1 × PBS and 1 mM TCEP) was dropped onto the AuE and incubated at 37 °C for 2 h. After rinsing, the AuE was immersed in 1 mM MCH for 30 min to minimize nonspecific adsorption. Subsequently, the activated Cas12a complex was applied to the electrode for 30 min at 37 °C for cleavage. The TdT-mediated extension was then performed by incubating the AuE with a mixture of TdT and dNTPs for 1 h at 37 °C. Finally, the electrode was incubated with 5 μL of hemin solution (200 μM in 20 mM HEPES, 50 mM KCl, 200 mM NaCl, 1% DMSO, pH 8.0) for 30 min at room temperature to form the G4/hemin complexes.

Electrochemical Measurements

Electrochemical impedance spectroscopy (EIS) and cyclic voltammetry (CV) were performed in 0.1 M KCl containing 5.0 mM $[Fe(CN)_6]^{3-/4-}$.[25] EIS was recorded from 0.1 Hz to 100 kHz with a 5.0 mV amplitude at a bias of 0.22 V vs SCE. Differential pulse voltammetry (DPV) was performed in electrolyte buffer (20 mM HEPES, 50 mM KCl, 200 mM NaCl, pH 8.0) from −0.1 to −0.6 V vs SCE with a pulse amplitude of 50 mV and a pulse width of 25 ms. All buffers were degassed with high-purity N_2 for 30 min to eliminate oxygen interference. Measurements were performed at 25 ± 2 °C.

Preparation of Spiked Milk Samples

Commercial whole milk was utilized as a complex matrix model.[26] Various concentrations of tetracycline (Tc) were spiked into milk for subsequent quantitative analysis using the developed biosensor. Briefly, 1.0 mL of above milk was mixed with 3.0 mL of anhydrous methanol (1:3, v/v) and vortexed for 60 s to precipitate proteins. After standing for 5 min, the mixture was centrifuged at 12,000 g for 15 min at 4 °C. The resulting supernatant was collected to serve as the sample.

RESULTS AND DISCUSSION

Verification of G4 Formation via TdT Extension Mediated by Cas12a *Trans*-Cleavage

The core of our sensing strategy hinges on the successful formation of G-quadruplex (G4) structures through Cas12a-mediated hairpin probe (Hp) cleavage, followed by TdT-catalyzed elongation (Figure 1A). Upon folding into G4 architectures, the TdT-generated G-rich sequences bind hemin to form G4/hemin complexes. These complexes act as electroactive centers on the electrode surface, facilitating the redox process of hemin to generate a "turn-on" electrochemical signal. This design not only circumvents the inherently high background signal typical of traditional "signal-off" CRISPR assays but also introduces additional layer of signal amplification to enhance the detection sensitivity. To rigorously establish the feasibility of this design, we systematically characterized the reaction process, from DNA strand elongation to structural folding and functional catalytic activity.

We first examined whether the Cas12a-cleaved Hp could serve as an effective primer for TdT-mediated extension. The *trans*-cleavage of Hp by the activated Cas12a RNP exposes a

https://doi.org/10.1021/acs.analchem.6c02971
Anal. Chem. XXXX, XXX, XXX−XXX

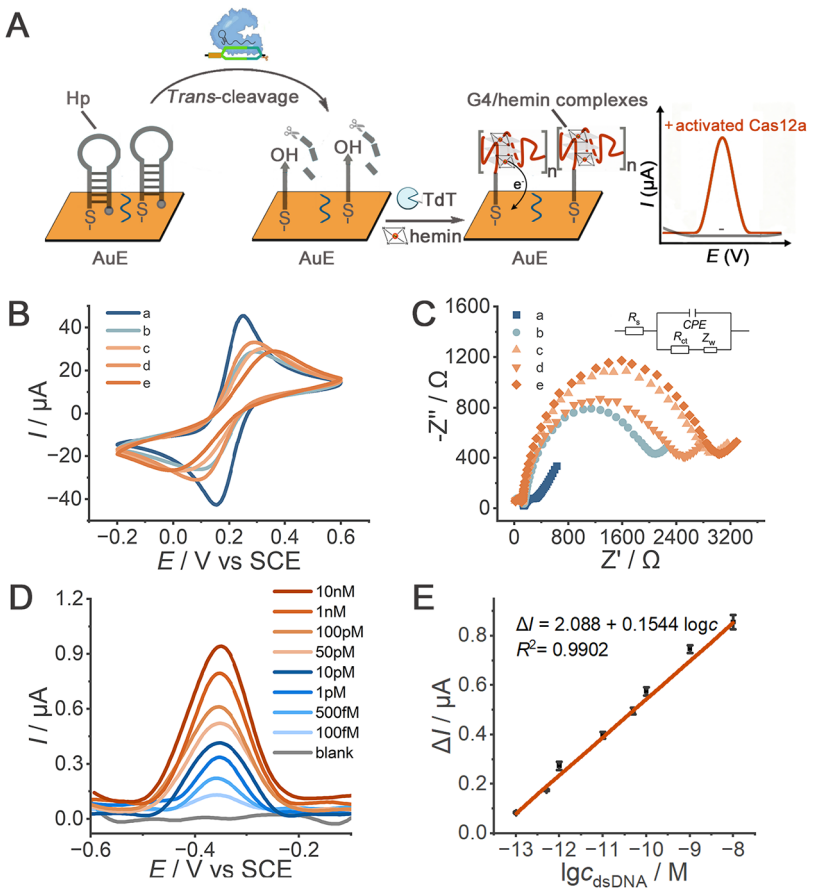


Figure 2. Construction and characterization of the label-free electrochemical interface. (A) Schematic representation of the stepwise assembly and signal generation process on the gold electrode (AuE). (B) Cyclic voltammograms (CV) and (C) electrochemical impedance spectra (EIS) recorded at various stages: (a) bare AuE, (b) Au/Hp, (c) Au/Hp/MCH, (d) Au/Hp/MCH/Cas12a, and (e) Au/Hp/MCH/Cas12a/TdT. (D) DPV responses of the biosensor toward different concentrations of dsDNA activators (0, 100 fM, 500 fM, 1 pM, 10 pM, 50 pM, 100 pM, 1 nM and 10 nM). (E) Linear relationship between the DPV peak current change (ΔI) and the logarithm of dsDNA concentration. ΔI is defined as $I-I_0$, where I and I_0 represent the DPV peak currents in the presence and absence of the target, respectively. Data are presented as mean ± SD (n = 3).

3′−OH terminus, which subsequently serves as a primer for TdT to initiate template-independent polymerization. Using an optimized dNTP mixture (10% dTTP, 40% dATP, and 50% dGTP) based on our previous study, TdT catalyzes the synthesis of long G-rich ssDNA. Native polyacrylamide gel electrophoresis (PAGE) was employed to characterize the reaction products. As shown in Figure 1B, Hp treated with activated Cas12a was successfully extended into DNA fragments several hundred bases in length (lane 5). In contrast, intact Hp failed to trigger extension because its 3′-hydroxyl group is blocked within the hairpin stem, thereby preventing TdT recognition (lane 3). Control experiments (Figure S1) demonstrated that no extension occurred in the absence of Hp, regardless of the presence of Cas12a RNP, verifying that the extension products originated exclusively from the cleaved Hp fragments.

While PAGE analysis confirmed the successful polymerization of DNA, it did not elucidate the secondary conformation of the synthesized long-chain products. Therefore, the structural configuration of the extension products was further characterized by circular dichroism (CD) spectroscopy. In the presence of K^+, the CD spectrum of the products exhibited a distinct negative peak at 240 nm and a dominant positive peak at 260 nm (Figure 1C), characteristic of a parallel G4 topology.[27−30] To provide further evidence of G4 folding in solution, thioflavin T (ThT) staining assays were conducted.[31,32] A significantly enhanced fluorescence signal was observed in the reaction group compared to the negligible background in the control groups (Figure 1D). Moreover, UV−vis absorption spectroscopy was further used to verify whether these folded G4 structures could effectively bind hemin to form G4/hemin complexes. The characteristic Soret band of hemin shifted from approximately 397 to 404 nm after incubation with the generated G4 structures, demonstrating the formation of G4/hemin complexes (Figure S2).[33] Finally, we evaluated the peroxidase-like activity of the resulting G4/hemin DNAzyme.[34] In the presence of H_2O_2 and TMB, the characteristic absorption spectrum of oxidized TMB (oxTMB, λmax ≈ 650 nm) was clearly observed (Figure 1E), indicating that the generated G4/hemin complexes retained peroxidase-like catalytic activity.[35,36] Collectively, these results robustly demonstrate that the Cas12a-mediated *trans*-cleavage of Hp triggers efficient TdT elongation to form functional G4 structures.

Construction and Characterization of the Label-Free Electrochemical Interface

The aforementioned solution-phase assays demonstrated that Cas12a *trans*-cleavage-mediated TdT elongation effectively facilitates the formation of G4 structures. To further bridge this methodology with electrochemical platforms, we investigated

https://doi.org/10.1021/acs.analchem.6c02971
Anal. Chem. XXXX, XXX, XXX−XXX

whether the activated Cas12a ribonucleoprotein (RNP) could efficiently transform hairpin DNA (Hp) immobilized on the electrode interface into G4/hemin complexes. This transformation generates a label-free electrochemical signal that enables the monitoring of CRISPR/Cas12a activity. To this end, Hp was first anchored onto the gold electrode surface via Au−S bond, followed by blocking nonspecific sites with 6-mercapto-1-hexanol (MCH).[37,38] Upon introducing activated Cas12a, the *trans*-cleavage of Hp exposes the 3′-hydroxyl group, which serves as a primer for TdT. In the presence of dNTP substrates, TdT facilitates the extension of G-rich sequences that subsequently fold into G4 structures. Following incubation with hemin, the newly synthesized G4 motifs specifically capture hemin to assemble electroactive complexes. This generates a characteristic and robust electrochemical signal originating from the hemin's redox couple (Figure 2A).

The stepwise assembly of the electrochemical interface was characterized by CV (Figure 2B) and EIS (Figure 2C). The bare gold electrode exhibited a pair of well-defined redox peaks (curve *a*), reflecting its intrinsic electron transfer efficiency. Following Hp immobilization (curve *b*) and MCH blocking (curve *c*), the redox peak currents decreased progressively, accompanied by a corresponding increase in the charge transfer resistance (R_{ct}) due to the increased steric hindrance and the insulating nature of the organic layer. Subsequent *trans*-cleavage by activated Cas12a reduced the steric hindrance, leading to a partial recovery of the redox peaks (curve *d*). However, following TdT elongation in the presence of dNTPs, the redox peaks diminished significantly once again (curve *e*). This signal suppression is attributed to the substantial increase in steric hindrance and electrostatic repulsion generated by the elongated, negatively charged G-rich strands. Consistently, the R_{ct} of the gold electrode increased from 78.79 Ω (curve *a*) to 2027.34 Ω (curve *b*) after Hp modification and further rose to 2881.97 Ω (curve *c*) after MCH blocking. A sharp decrease in R_{ct} to 2548.46 Ω (curve *d*) was observed following Cas12a cleavage, while the subsequent TdT elongation resulted in a significant increase in R_{ct} to approximately 2975.51 Ω (curve *e*).

With the successful construction of the sensing interface confirmed, key parameters governing the sensor performance were systematically optimized. First, the grafting density of Hp on the electrode is critical for both Cas12a cleavage efficiency and subsequent TdT-mediated signal amplification. As shown in Figure S3, the DPV signal intensity increased significantly as the Hp concentration was raised from 0.1 μM to 2 μM, peaking at 2 μM. A further increase to 3 μM led to a decline in signal, suggesting that an excessively high probe density limits the accessibility of Cas12a to the cleavage site and inhibits TdT elongation efficiency due to severe steric crowding on the electrode surface. To balance sensitivity and stability, 2 μM was selected as the optimal immobilization concentration. Next, the *trans*-cleavage time for Cas12a was evaluated (Figure S4). The signal increased steadily up to 0.5 h but declined thereafter, likely due to the gradual nonspecific detachment of probes from the electrode or minor degradation over prolonged incubation; thus, 0.5 h was identified as the optimal cleavage time. Furthermore, the duration of TdT elongation showed a positive correlation with the DPV signal from 0.25 to 1.0 h, reaching a plateau after 1.0 h (Figure S5). This plateau indicates that the extension reaction had reached a state of steric saturation at the solid−liquid interface. To balance detection efficiency with sensitivity, 1.0 h was chosen as the optimal extension time. Finally, an investigation of the pH effect revealed the strongest electrochemical response at pH 8.0 (Figure S6), which is consistent with the high biological activity of TdT and Cas12a in slightly alkaline environments. Consequently, these optimized parameters were adopted as standard conditions for all subsequent experiments.

Having established the structural integrity and optimal operational conditions of the sensing interface, we proceeded to quantitatively evaluate its analytical performance. Given that double-stranded DNA (dsDNA) serves as the inherent activator for the Cas12a system, we first employed a synthetic dsDNA as a model target to directly trigger the Cas12a *trans*-cleavage activity. This direct activation circumvents the need for upstream aTF modules, thereby providing a straightforward baseline to validate the signal transduction efficiency. We monitored current changes via differential pulse voltammetry (DPV) to establish the assay's sensitivity. As shown in Figure 2D, the DPV peak at approximately −0.35 V increased proportionally as the target dsDNA concentration rose from 100 fM to 10 nM. The response signal exhibited a strong linear relationship with the logarithm of the dsDNA concentration (Figure 2E), yielding a limit of detection (LOD) of approximately 42 fM based on the classical 3σ criterion.[7] This sensitivity significantly outperforms that of traditional CRISPR-based fluorescence assays (the lowest detectable concentration, 50 pM) conducted under similar conditions (Figure S7). These findings demonstrate the successful construction of a label-free, "turn-on" electrochemical interface for reporting Cas12a activity, characterized by high sensitivity afforded by the dual-stage amplification of Cas12a cleavage and TdT extension. Crucially, this impressive analytical performance validates the platform's capability to trace low abundance targets, setting a robust foundation for the subsequent integration of aTF modules for small-molecule sensing.

TF-Cas12a Communication-Driven Label-Free Electrochemical Biosensor for Sensitive Small Molecule Detection

As demonstrated in the preceding section, the activated Cas12a RNP can efficiently cleave the Hp immobilized on the electrode surface, initiating a cascade that yields G4/hemin complexes and generates a detectable electrochemical signal. While our initial validation focused on the high-sensitivity detection of nucleic acid targets—leveraging their inherent sequence programmability for direct Cas12a activation—the detection of non-nucleic acid targets is equally critical for the food safety industry. Unlike nucleic acids, non-nucleic acid targets typically lack predictable sequence information for direct amplification and exhibit high structural diversity and distinct chemical properties. These attributes pose significant challenges for the direct adaptation of traditional nucleic acid-driven CRISPR strategies, thereby demanding more sophisticated signal transduction mechanisms and molecular recognition modules. To bridge this gap, we integrated a target-responsive nucleic acid transduction module, whereby recognition events of non-nucleic acid targets (e.g., small molecules) can be effectively converted into the functional activation of Cas12a. In this modular design, the target triggers a conformational change or molecular dissociation within the transduction unit, thereby unmasking the Cas12a-recognition DNA sequence from a previously sterically hindered state. Subsequently, the activated Cas12a RNP efficiently transforms the electrode-tethered Hp into G4/hemin complexes, produc-

https://doi.org/10.1021/acs.analchem.6c02971
Anal. Chem. XXXX, XXX, XXX−XXX

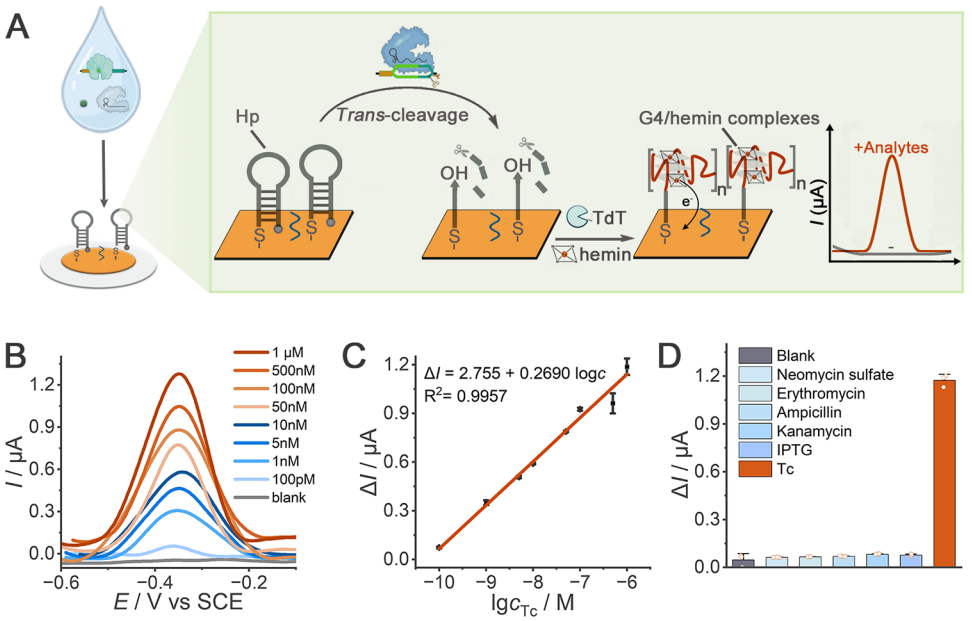


Figure 3. TF-Cas12a Communication-Driven Label-Free Electrochemical Biosensor for Sensitive Small Molecule Detection. (A) Schematic mechanism of the TetR-gated CRISPR/Cas12a System for label-free electrochemical detection of Tc. (B) DPV curves of the biosensor in response to various concentrations of Tc (blank, 100 pM, 1 nM, 5 nM, 10 nM, 50 nM, 100 nM, 500 nM and 1 μM). (C) Calibration curve showing the linear correlation between ΔI and the logarithm of Tc concentration from 100 pM to 1 μM. (D) Selectivity of the biosensor for Tc (500 nM) against other antibiotics and IPTG (each at 5 μM). Data are presented as mean ± SD (n = 3).

ing a measurable electrochemical signal. This modular design endows the sensing platform with high versatility, extending its applicability from nucleic acid targets to a broad range of small-molecule analytes.

To validate this modular concept in a practical scenario, we targeted antibiotic residues, which represent a high-priority chemical risk in food safety. Tetracycline (Tc) is a representative antibiotic that can be selectively recognized by the specific transcription factor TetR (Figure S8), a binding process accompanied by significant protein conformational changes.[39−41] Building upon the principle of ligand-responsive TF-Cas12a communication, we developed a label-free "turn-on" biosensor for Tc detection by incorporating TetR, the tetracycline operator (TetO) sequence, and Cas12a into the transduction module.[8] To construct this sensing cascade, we initially designed a dsDNA adaptor containing two functional domains: a PAM and protospacer sequence for Cas12a recognition, and a TetO sequence for TetR binding. In the absence of Tc, TetR specifically binds to the TetO site on the DNA. Due to its substantial molecular bulk, the bound TetR exerts severe steric hindrance that blocks the Cas12a-crRNA complex from binding to the adjacent protospacer DNA. Consequently, Cas12a remains inactive, lacking *trans*-cleavage activity and yielding no electrochemical signal. Conversely, in the presence of Tc, the antibiotic binds to TetR, inducing a conformational change that triggers the dissociation of TetR from the DNA. The exposed DNA sequence then freely recruits the Cas12a RNP, activating its high-efficiency cleavage of Hp into G4/hemin complexes and generating a detectable signal (Figure 3A). To validate the feasibility of this platform for Tc detection, we compared the signal responses in the presence and absence of the target (Figure S9). In the blank control group, the negligible electrochemical signal and extremely low background current confirmed that Cas12a remained strictly inactive and subsequent TdT-mediated amplification was prevented. In contrast, the introduction of 50 nM Tc elicited a robust electrochemical response. This distinct "off-to-on" signal transition strongly demonstrates the high feasibility of this sensing strategy for Tc detection.

Subsequently, we evaluated the biosensor's quantitative performance across varying Tc concentrations. As the Tc concentration increased from 100 pM to 1 μM, the DPV peak currents exhibited a gradual rise (Figure 3B). A strong linear relationship was observed between the DPV peak current (ΔI) and the logarithm of the Tc concentration (ranging from 100 pM to 1 μM), described by the regression equation: ΔI = 2.755 + 0.2690 lg c (R^2 = 0.9957), yielding a LOD reaching 36 pM (Figure 3C). To evaluate the sensor's reliability, intra-assay assessments across six biosensors from the same batch were performed, showing high consistency (Figure S10A). Furthermore, interassay analysis of six different batches under identical conditions yielded a relative standard deviation (RSD) of only 6.7% (Figure S10B), demonstrating the excellent reproducibility of this biosensor. By integrating the CRISPR/Cas system with an electrochemical interface, we have developed a platform capable of pM-level sensitivity for small-molecule detection, which significantly improved the detection sensitivity compared to many previously reported biosensing methods (Table S3). Notably, as shown in Figure 3D, no significant current changes were observed when the platform was exposed to other antibiotics and small-molecule interferents (including neomycin sulfate, erythromycin, ampicillin, kanamycin and IPTG), highlighting its superior selectivity attributable to the specific ligand-binding cavity of TetR. In summary, we constructed a sensitive CRISPR/Cas12a-based electrochemical sensing platform regulated by the transcription factor TetR for the "turn-on" detection of Tc.

Versatility of the Modular Sensing Platform Across Diverse Analytes

Following the successful construction of sensing platforms for nucleic acids and tetracycline, we sought to further validate the

https://doi.org/10.1021/acs.analchem.6c02971
Anal. Chem. XXXX, XXX, XXX−XXX

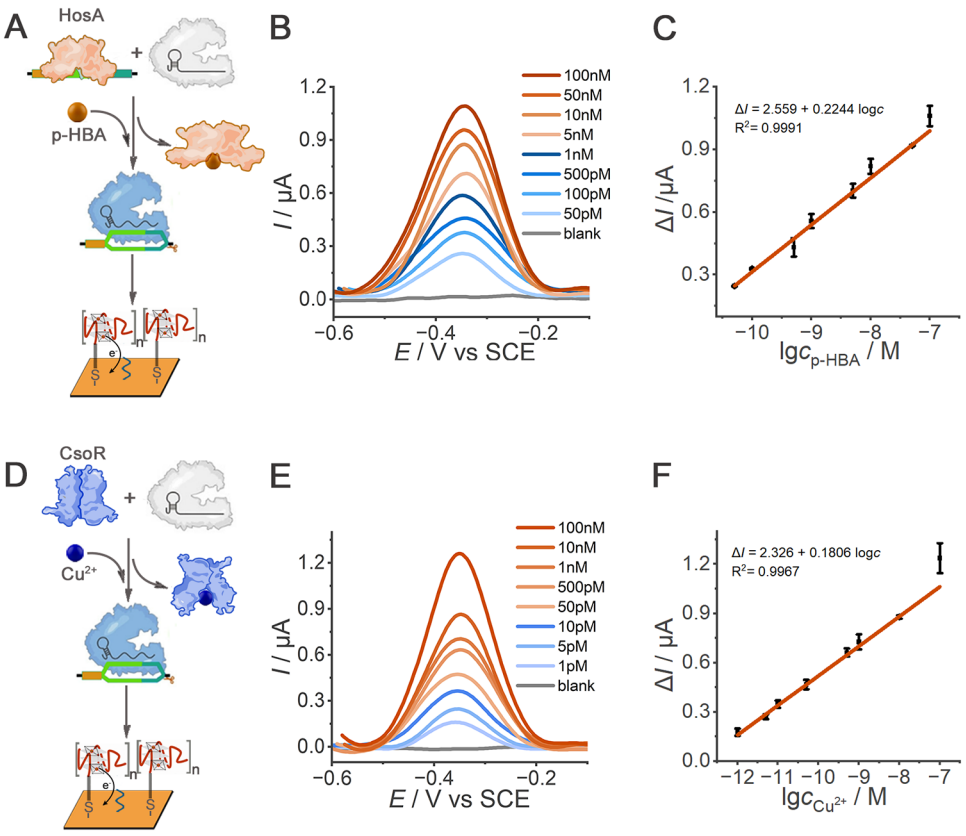


Figure 4. Versatility of the Modular Sensing Platform Across Diverse Analytes. (A) Schematic of *p*-hydroxybenzoic acid (*p*-HBA) detection based on the HosA-gated module. (B) DPV responses and (C) the corresponding linear fitting curve for *p*-HBA (ranging from 50 pM to 100 nM). (D) Schematic of Cu^{2+} detection regulated by the CsoR transcription factor. (E) DPV responses and (F) the corresponding linear fitting curve for Cu^{2+} detection (ranging from 1 pM to 100 nM). Data are presented as mean ± SD (n = 3).

potential of this TF-gated CRISPR strategy as a universal biosensing framework. The modularity of our design enables the seamless expansion of the target scope by simply substituting the aTFs and their corresponding nucleic acid sequences within the transduction module, while maintaining the downstream CRISPR/Cas12a-TdT signal transduction and amplification modules intact. This allows the platform to accommodate analytes with vastly different structural and chemical properties, ranging from aromatic organic compounds to inorganic metal ions.

Food preservatives are indispensable additives in the modern food industry, primarily used to inhibit the growth of microorganisms (bacteria, fungi, and yeast), thereby delaying spoilage and reducing food waste.[42,43] However, their overuse, illegal addition, and long-term cumulative effects pose potential threats to human health. Among these, *p*-hydroxybenzoic acid (*p*-HBA) has garnered considerable attention due to its widespread application and potential endocrine-disrupting properties.[10,44] Despite its antimicrobial efficacy, its structural similarity to estrogen has raised concerns regarding reproductive toxicity and carcinogenicity, making the rapid and sensitive monitoring of *p*-HBA residues a priority for food safety regulation. Consequently, we selected *p*-HBA as a model target and integrated its corresponding transcription factor, HosA (Figure S8), to evaluate the platform's adaptability to aromatic preservatives (Figure 4A). Consistent with the previously described system, the engineered dsDNA contains a PAM−protospacer region for Cas12a recognition and a regulatory sequence for specific HosA binding. In the absence of *p*-HBA, HosA specifically binds to the dsDNA, acting as a molecular gate to block Cas12a activation and resulting in a negligible electrochemical signal. Conversely, the introduction of *p*-HBA triggers HosA dissociation, thereby unblocking the target DNA for the Cas12a/crRNA complex. The exposed DNA adaptor was then recognized by the preassembled Cas12a/crRNA RNP, thereby activating its *trans*-cleavage activity. The activated Cas12a efficiently cleaves the electrode-immobilized Hp, which subsequently facilitates the formation of electrocatalytically active G4/hemin complexes to generate an electrochemical signal. DPV measurements across varying *p*-HBA concentrations showed that the peak current increased progressively with target concentration, exhibiting a robust linear response from 50 pM to 100 nM (Figure 4B). The linear regression equation was determined as $\Delta I = 2.559 + 0.2244 \lg c$ ($R^2 = 0.9991$), yielding a LOD as low as 45 pM and confirming the platform's capability for the sensitive detection of aromatic small molecules (Figure 4C). To further assess the selectivity of the HosA-gated sensing module, structurally related aromatic compounds and preservatives, including benzoic acid, *p*-hydroxybenzaldehyde, salicylic acid, *p*-hydroxyphenylacetic acid, and 3,4-dihydroxybenzoic acid, were tested as potential interferents. Notably, these interferents were examined at a 10-fold higher concentration than *p*-HBA to provide a stringent selectivity evaluation. As shown in Figure S11A, only *p*-HBA produced a pronounced DPV response, whereas the structurally related compounds induced negligible current changes. These results demonstrate that the HosA-gated module retains good target selectivity even in the

https://doi.org/10.1021/acs.analchem.6c02971
Anal. Chem. XXXX, XXX, XXX−XXX

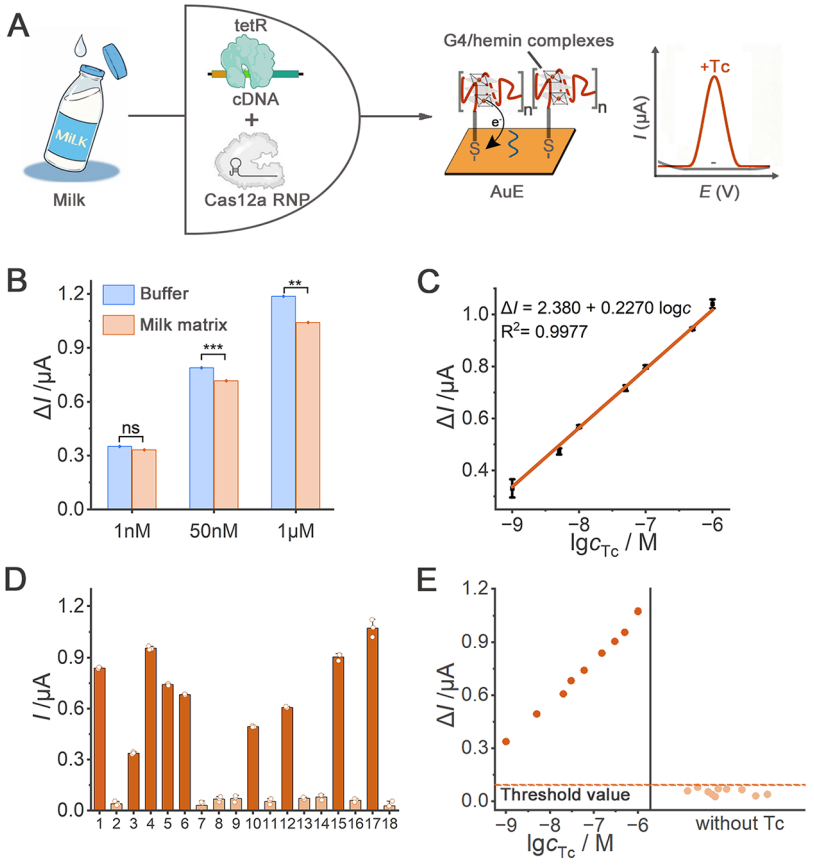


Figure 5. Detection of Tetracycline in Real Milk Samples. (A) Schematic mechanism of Tc detection in milk samples. (B) Comparison of the DPV peak current changes (ΔI) for Tc (1 nM, 50 nM, and 1 μM) in buffer and pretreated milk matrix. Data are presented as mean ± SD (n = 3). Statistical significance was assessed by two-tailed Student's t test. ns, not significant ($P \geq 0.05$); **$P < 0.01$; ***$P < 0.001$. (C) Matrix-matched calibration curve for Tc in milk matrix (ranging from 1 nM to 1 μM). Data are presented as mean ± SD (n = 3). (D) DPV signal response of blind samples and (E) Scatter plot of the DPV signals for blind samples; the dashed line represents the threshold for differentiating positive and negative samples, which was defined as the mean plus 3-fold standard deviation of the negative control.

presence of closely related aromatic interferents, which can be attributed to the specific ligand-responsive behavior of HosA.

To further push the boundaries of this modular architecture beyond organic compounds, we selected copper ions (Cu^{2+})—a representative heavy metal prevalent in environmental and industrial water samples, characterized by high toxicity and strict regulatory limits—to further verify the platform's versatility.[45−47] By introducing the corresponding transcription factor CsoR (Figure S8) and its specific DNA recognition sequence, we constructed a label-free "turn-on" electrochemical biosensor for Cu^{2+} detection, utilizing a conformational switch induced by metal coordination (Figure 4D).[48] Under optimized conditions, the DPV peak current increased as the Cu^{2+} concentration rose from 1 pM to 100 nM (Figure 4E). A linear relationship was observed between the DPV peak current (ΔI) and the logarithm of the Cu^{2+} concentration, yielding the regression equation: $\Delta I = 2.326 + 0.1806 \lg c$ (R^2 = 0.9967), with the LOD of 0.33 pM (Figure 4F). Furthermore, the ion selectivity of the CsoR-based sensing module was assessed by exposing the platform to various potentially interfering metal ions, including Ba^{2+}, Ca^{2+}, Fe^{2+}, Mn^{2+}, Ni^{2+}, and Zn^{2+}. As shown in Figure S11B, these competing metal ions caused no appreciable current changes, confirming the excellent selectivity of the platform, which can be attributed to the specific copper-responsive regulatory behavior of CsoR. These results demonstrate the platform's efficacy for the sensitive quantification of metal ions.

Collectively, these experimental data indicate that the developed electrochemical sensing system can achieve effective recognition and robust signal output for targets with vastly different structural and chemical attributes by simply swapping the transcription factors within the nucleic acid transduction module. This further validates the excellent universality of our design strategy. By replacing or customizing specific TF−operator pairs, this platform holds significant promise for expansion to a broader array of small molecules and ionic analytes, providing a versatile and efficient solution for environmental monitoring and food safety applications.

Detection of Tetracycline in Real Milk Samples

To evaluate the practical application potential of the developed assay in complex real-world matrices, milk was selected as a representative substrate for validation (Figure 5A). Given its high consumption as a staple food, milk is a primary target for food safety monitoring due to the potential risk of antibiotic residues originating from the production process.[49] However, the complex components in milk, such as proteins and lipids, can cause nonspecific interference with molecular recognition and subsequent signal transduction. Therefore, achieving stable and reliable antibiotic detection in a milk matrix is critical for verifying the anti-interference capability and practical applicability of the proposed method.

https://doi.org/10.1021/acs.analchem.6c02971
Anal. Chem. XXXX, XXX, XXX−XXX

Given the complexity of the milk matrix, we evaluated the reliability of the sensor through matrix-matching experiments. Tetracycline (Tc) at gradient concentrations (1 nM, 50 nM, and 1 μM) was spiked into both buffer and milk samples. The selected concentrations, 1 nM, 50 nM, and 1 μM, represent the low, middle, and high regions of the matrix-matched linear range, respectively. The milk samples were initially pretreated via degreasing and protein precipitation to minimize electrochemical interference from endogenous substances. Subsequently, signal responses in the buffer and pretreated milk matrix were compared. Compared to the buffer system, the milk matrix caused signal attenuation across all tested concentrations (Figures 5B and S12). This attenuation likely stems from residual matrix components interfering with the electrode interface or the enzymatic activity of Cas12a/TdT, underscoring the presence of a non-negligible matrix effect. Consequently, it was necessary to re-establish the quantitative relationship for Tc within the milk matrix to ensure accurate quantification. Thus, a matrix-matched calibration curve was constructed. The experimental data revealed a robust linear response for Tc in milk over the concentration range of 1 nM to 1 μM (Figure S13). The linear regression equation was determined as $\Delta I = 2.380 + 0.2270 \lg c$ ($R^2 = 0.9977$) demonstrating the stable quantitative capability of this method even in a complex milk matrix (Figure 5C).

To further assess the accuracy and discriminative performance of the method for practical applications, we conducted a randomized blind test. A series of milk samples, including both negative and spiked positive samples, were numbered (1−18), with the actual identities of the samples blinded to the analyst. Notably, all spiking occurred prior to pretreatment to ensure a consistent matrix environment throughout the detection workflow. The blind test results (Figure 5D) showed accurate identification of all 9 negative samples without any false-positive signals. Conversely, the electrochemical responses for the 9 spiked positive samples (ranging from 1 nM to 1 μM) were in good agreement with the matrix-matched calibration curve, clearly differentiating them from the negative group (Figure 5E). This accurate identification of unknown samples strongly demonstrates the method's excellent reliability and confirms that the combination of sample pretreatment and a matrix-matching strategy effectively overcomes nonspecific interference from the milk matrix. Therefore, this work provides a viable strategy for the sensitive monitoring of antibiotic residues in complex matrices, demonstrating significant potential in the field of food safety.

CONCLUSIONS

In conclusion, we developed a highly modular and sensitive label-free electrochemical biosensing platform that couples aTF recognition with a CRISPR/Cas12a and TdT dual-amplification cascade. By converting target-induced aTF dissociation into Cas12a activation, the system triggers the TdT-mediated elongation of cleaved hairpin probes into electroactive G4/hemin complexes. This unique "turn-on" signal transduction mechanism not only circumvents the high background currents typical of traditional "signal-off" CRISPR assays but also achieves exceptional signal enhancement. The proposed sensor exhibited excellent analytical performance across structurally diverse analytes, yielding picomolar-level limits of detection for tetracycline (36 pM), *p*-hydroxybenzoic acid (45 pM), and copper ions (0.33 pM). Furthermore, the practical utility of the assay was validated in complex milk matrices. By employing a matrix-matched calibration strategy, the sensor effectively overcame endogenous interference, demonstrating high accuracy and reliability in randomized blind testing. Importantly, the "plug-and-play" architecture of the transduction module enables seamless adaptation to a wide range of organic and inorganic targets through the simple substitution of specific TF-operator pairs. This highly versatile and robust biosensing methodology provides a powerful analytical tool for the ultrasensitive monitoring of antibiotic residues, food preservatives, and heavy metal pollutants, holding significant promise for broad implementation in food safety regulation and environmental diagnostics.

ASSOCIATED CONTENT

Supporting Information

The Supporting Information is available free of charge at https://pubs.acs.org/doi/10.1021/acs.analchem.6c02971.

Detailed description of the experimental procedures; nucleic acid sequence and preparation; fluorometric measurements; reproducibility of this biosensor; optimization of reaction conditions; and more detailed results (PDF)

AUTHOR INFORMATION

Corresponding Authors

Yan Huang − *State Key Laboratory of Chemo and Biosensing, College of Chemistry and Chemical Engineering, Hunan Provincial Key Laboratory of Biomacromolecular Chemical Biology, Hunan University, Changsha 410082, P. R. China;* orcid.org/0000-0001-5965-5739; Email: yanhuang@hnu.edu.cn

Chunyang Lei − *State Key Laboratory of Chemo and Biosensing, College of Chemistry and Chemical Engineering, Hunan Provincial Key Laboratory of Biomacromolecular Chemical Biology, Hunan University, Changsha 410082, P. R. China;* orcid.org/0000-0002-3078-5553; Email: cylei@hnu.edu.cn

Authors

Liang Zhu − *State Key Laboratory of Chemo and Biosensing, College of Chemistry and Chemical Engineering, Hunan Provincial Key Laboratory of Biomacromolecular Chemical Biology, Hunan University, Changsha 410082, P. R. China*

Lejun Liao − *State Key Laboratory of Chemo and Biosensing, College of Chemistry and Chemical Engineering, Hunan Provincial Key Laboratory of Biomacromolecular Chemical Biology, Hunan University, Changsha 410082, P. R. China*

Zhou Nie − *State Key Laboratory of Chemo and Biosensing, College of Chemistry and Chemical Engineering, Hunan Provincial Key Laboratory of Biomacromolecular Chemical Biology, Hunan University, Changsha 410082, P. R. China;* orcid.org/0000-0001-9864-2965

Complete contact information is available at: https://pubs.acs.org/10.1021/acs.analchem.6c02971

Author Contributions

This manuscript was written with the contributions of all authors. All authors have given approval to the final version of the manuscript.

Notes

The authors declare no competing financial interest.

https://doi.org/10.1021/acs.analchem.6c02971
Anal. Chem. XXXX, XXX, XXX−XXX

■ ACKNOWLEDGMENTS

This work was supported by the National Natural Science Foundation of China (22374036, 22422404, and 22274041) and the National Natural Science Foundation of Hunan Province (2023ZJ1120).

■ REFERENCES

(1) Hu, H.; Guo, S.; Li, Y.; Dong, K.; Lu, Y.; Ye, K.; Li, L.; Zhou, X.; Cheng, L.; Xiao, X. Spatially Blocked Split CRISPR-Cas12a System for Ultra-Sensitive and Versatile Small Molecule Activation and Detection. *Nat. Commun.* **2025**, *16* (1), No. 5035.

(2) Wu, H.; Eckhardt, C. M.; Baccarelli, A. A. Molecular Mechanisms of Environmental Exposures and Human Disease. *Nat. Rev. Genet.* **2023**, *24* (5), 332−344.

(3) Chen, J. S.; Ma, E.; Harrington, L. B.; Da Costa, M.; Tian, X.; Palefsky, J. M.; Doudna, J. A. CRISPR-Cas12a Target Binding Unleashes Indiscriminate Single-Stranded DNase Activity. *Science* **2018**, *360* (6387), 436−439.

(4) Avaro, A. S.; Griffiths, A. D.; Santiago, J. G. Degradation of Reporter Molecules Imposes a Fundamental Limit of Detection on CRISPR Diagnostics. *Anal. Chem.* **2025**, *97* (25), 13192−13200.

(5) Cao, L.; Wang, Z.; Lei, C.; Nie, Z. Engineered CRISPR/Cas Ribonucleoproteins for Enhanced Biosensing and Bioimaging. *Anal. Chem.* **2025**, *97* (11), 5866−5879.

(6) Di Pede, A. C.; Bagheri, N.; Belforte, E.; Palone, A.; Rossetti, M.; Porchetta, A. Triplex DNA Clamp Regulates Cas12a Activation for ssDNA and RNA Sensing. *Nucleic Acids Res.* **2026**, *54* (1), No. gkaf1392.

(7) Zhang, T.; Zhao, Y.; Zhu, C.; Zhu, X.; Zhu, X.; Qiu, Y.; Nie, Z.; Lei, C. CRISPR/Cas12a Protein Switch Powered Label-Free Electrochemical Biosensor for Sensitive Viral Protease Detection. *Anal. Chem.* **2025**, *97* (14), 8039−8047.

(8) Wang, K.; Liu, S.; Zhou, S.; Qileng, A.; Wang, D.; Liu, Y.; Chen, C.; Lei, C.; Nie, Z. Ligand-Responsive Artificial Protein−Protein Communication for Field-Deployable Cell-Free Biosensing. *Angew. Chem., Int. Ed.* **2025**, *64* (4), No. e202416671.

(9) Capelli, L.; Marzari, S.; Spezzani, E.; Bertucci, A. Synthetic CRISPR Networks Driven by Transcription Factors via Structure-Switching DNA Translators. *J. Am. Chem. Soc.* **2025**, *147* (24), 21184−21193.

(10) Liang, M.; Li, Z.; Wang, W.; Liu, J.; Liu, L.; Zhu, G.; Karthik, L.; Wang, M.; Wang, K.; Wang, Z.; Yu, J.; Shuai, Y.; Yu, J.; Zhang, L.; Yang, Z.; Li, C.; Zhang, Q.; Shi, T.; Zhou, L.; Xie, F.; Dai, H.; Liu, X.; Zhang, J.; Liu, G.; Zhuo, Y.; Zhang, B.; Liu, C.; Li, S.; Xia, X.; Tong, Y.; Liu, Y.; Alterovitz, G.; Tan, G.-Y.; Zhang, L. A CRISPR-Cas12a-Derived Biosensing Platform for the Highly Sensitive Detection of Diverse Small Molecules. *Nat. Commun.* **2019**, *10* (1), No. 3672.

(11) Yin, L.; Zhou, C.; Gao, B.; Liu, F.; Ma, L.; Guo, F. Engineering CRISPR/Cas12-Based Biosensors: Recent Advances and Future Perspectives. *TrAC Trends Anal. Chem.* **2025**, *191*, No. 118296.

(12) Aliev, T. A.; Belyaev, V. E.; Pomytkina, A. V.; Nesterov, P. V.; Shityakov, S.; Sadovnichii, R. V.; Novikov, A. S.; Orlova, O. Yu.; Masalovich, M. S.; Skorb, E. V. Electrochemical Sensor to Detect Antibiotics in Milk Based on Machine Learning Algorithms. *ACS Appl. Mater. Interfaces* **2023**, *15* (44), 52010−52020.

(13) Luo, J.; Zhu, Z. Sensitive and High-Throughput Time-Resolved Luminescence Detection of Tetracycline in Milk for Eliminating Background Fluorescence on a Miniaturized Apparatus. *Anal. Chem.* **2024**, *96* (28), 11115−11120.

(14) Duan, M.; Li, G.; Shen, J.; Dai, R.; Li, X.; Liu, Z.; Jia, F. A CRISPR/Cas12a Biosensor for Portable and Accessible Detection of *Salmonella Typhimurium* via Multi-Indicator pH Millidisc Colorimetry and Smartphone Imaging Platform. *Biosens. Bioelectron.* **2025**, *286*, No. 117611.

(15) Zhao, J.; Cheng, S.; Wang, X.; Yu, R.; Du, B.; Tong, J.; Liu, Y.; Qing, T.; Liu, X. Urease-Mediated Homogeneous Dual-Mode Biosensor for on-Site Qualitative and Accurate Sensitive Quantitative Detection of Toxic Soluble Aβ Oligomers in Undiluted Samples. *Chem. Eng. J.* **2025**, *521*, No. 166632.

(16) Song, J.; Xu, C.; Zeng, S.; Zuo, W.; Yang, Q.; Hu, Q.; Meng, X.; Ye, J.; Dai, J.; Ju, Y. Metal Ion-Based Chemical Coordination Amplification: A Chromophore In Situ Deposition Strategy for Visual Sensitivity-Enhanced Lateral Flow Immunochromatography Assays. *Anal. Chem.* **2025**, *97* (6), 3477−3485.

(17) Sena-Torralba, A.; Álvarez-Diduk, R.; Parolo, C.; Piper, A.; Merkoçi, A. Toward Next Generation Lateral Flow Assays: Integration of Nanomaterials. *Chem. Rev.* **2022**, *122* (18), 14881−14910.

(18) Chu, M.; Zhang, Y.; Ji, C.; Zhang, Y.; Yuan, Q.; Tan, J. DNA Nanomaterial-Based Electrochemical Biosensors for Clinical Diagnosis. *ACS Nano* **2024**, *18* (46), 31713−31736.

(19) Bracaglia, S.; Ranallo, S.; Ricci, F. Electrochemical Cell-Free Biosensors for Antibody Detection. *Angew. Chem., Int. Ed.* **2023**, *62* (8), No. e202216512.

(20) Ji, D.; Guo, M.; Wu, Y.; Liu, W.; Luo, S.; Wang, X.; Kang, H.; Chen, Y.; Dai, C.; Kong, D.; Ma, H.; Liu, Y.; Wei, D. Electrochemical Detection of a Few Copies of Unamplified SARS-CoV-2 Nucleic Acids by a Self-Actuated Molecular System. *J. Am. Chem. Soc.* **2022**, *144* (30), 13526−13537.

(21) Guo, Y.; Guo, W.; Wu, Z.; Xu, H.; Zhang, X.; Zou, X.; Sun, Z. A Microfluidic Chip-Based Electrochemical Biosensor Coupled with CRISPR/Cas12a for Simultaneous Detection of Foodborne Pathogens. *Anal. Chem.* **2025**, *97* (49), 27266−27275.

(22) Dai, Y.; Somoza, R. A.; Wang, L.; Welter, J. F.; Li, Y.; Caplan, A. I.; Liu, C. C. Exploring the Trans-Cleavage Activity of CRISPR-Cas12a (Cpf1) for the Development of a Universal Electrochemical Biosensor. *Angew. Chem., Int. Ed.* **2019**, *58* (48), 17399−17405.

(23) Zhao, J.; Kong, D.; Zhang, G.; Zhang, S.; Wu, Y.; Dai, C.; Chen, Y.; Yang, Y.; Liu, Y.; Wei, D. An Efficient CRISPR/Cas Cooperative Shearing Platform for Clinical Diagnostics Applications. *Angew. Chem., Int. Ed.* **2024**, *63* (52), No. e202411705.

(24) Yuan, X.; Xu, Y.; Zhang, G.; Wang, Y.; Jin, X. CRISPR/Cas12a-Mediated Electrochemical Aptasensor for Simultaneous Determination of Alzheimer's Disease Biomarkers in Human Blood. *Anal. Chem.* **2025**, *97* (32), 17715−17724.

(25) Budak, F.; Cetinkaya, A.; Unal, M. A.; Ozkan, S. A. Design of Molecularly Imprinted Polymer Based Electrochemical Sensor for Eco-Friendly, Selective, and Sensitive Determination of Lincomycin in Food Samples. *Food Chem.* **2025**, *488*, No. 144883.

(26) Yuan, H.-Q.; Yang, Q.; Guo, L.; Wang, Y.; Li, G.; Cui, Q.; Dou, Z.; Cai, Z.; Xia, Y.; Bao, G. New Meso-porous UiO-66-OH Framework with in-Situ Grown $CsPbBr_3$ Perovskite Nanocrystals as a Multifunctional Sensor for the Discrimination and Instrument-Free Detection of Three Natural Food Additives. *Chem. Eng. J.* **2026**, *537*, No. 176367.

(27) Li, X.; Zheng, J.; Fang, X.; Gao, W.; Chen, H.; Liu, Z.; Li, C.; Zhang, R. Multiple microRNAs Analysis Based on DNAzyme Cascade DNA Fiber Barcodes for Cell Typing. *Biosens. Bioelectron.* **2026**, *297*, No. 118383.

(28) Geng, Y.; Liu, C.; Miao, H.; Suen, M. C.; Xie, Y.; Zhang, B.; Han, W.; Wu, C.; Ren, H.; Chen, X.; Tai, H.; Wang, Z.; Zhu, G.; Cai, Q. Crystal Structures of Distinct Parallel and Antiparallel DNA G-Quadruplexes Reveal Structural Polymorphism in C9orf72 G4C2 Repeats. *Nucleic Acids Res.* **2025**, *53* (17), No. gkaf879.

(29) Wang, Y.; Wang, J.; Yan, Z.; Hou, J.; Wan, L.; Yang, Y.; Liu, Y.; Yi, J.; Guo, P.; Han, D. Structural Investigation of Pathogenic RFC1 AAGGG Pentanucleotide Repeats Reveals a Role of G-Quadruplex in Dysregulated Gene Expression in CANVAS. *Nucleic Acids Res.* **2024**, *52* (5), 2698−2710.

(30) Lv, M.; Ren, J.; Wang, E. Topological Effect of an Intramolecular Split G-Quadruplex on Thioflavin T Binding and Fluorescence Light-Up. *Chem. Sci.* **2024**, *15* (12), 4519−4528.

(31) Hu, J.; Zhang, X.; Cao, H.; Zhang, C. Modular Engineering of a Hierarchical Hybridization-Reconfiguration-Replication Circuit for Rapid Detection of Long Noncoding RNA with Attomolar Sensitivity. *Chem. Eng. J.* **2023**, *474*, No. 145746.

(32) Zhang, Z.-k.; Jing, S.; Cao, S.; Zhang, N.; Li, C.; Luo, X. Dual Cascade Signal Amplification Lights up G4 Dimers for Fluorescent

https://doi.org/10.1021/acs.analchem.6c02971
Anal. Chem. XXXX, XXX, XXX−XXX

Detection of DNA Repair Enzyme FEN1. *Biosens. Bioelectron.* **2026**, *292*, No. 118077.
(33) Li, W.; Li, Y.; Liu, Z.; Lin, B.; Yi, H.; Xu, F.; Nie, Z.; Yao, S. Insight into G-Quadruplex-Hemin DNAzyme/RNAzyme: Adjacent Adenine as the Intramolecular Species for Remarkable Enhancement of Enzymatic Activity. *Nucleic Acids Res.* **2016**, *44* (15), 7373−7384.
(34) Zhang, X.; Qiu, D.; Chen, J.; Zhang, Y.; Wang, J.; Chen, D.; Liu, Y.; Cheng, M.; Monchaud, D.; Mergny, J.; Ju, H.; Zhou, J. Chimeric Biocatalyst Combining Peptidic and Nucleic Acid Components Overcomes the Performance and Limitations of the Native Horseradish Peroxidase. *J. Am. Chem. Soc.* **2023**, *145* (8), 4517−4526.
(35) Bi, W.; Cao, X.; Li, J.; Gao, Y.; Song, Y.; He, B. Ultrasensitive Detection of Extracellular Vesicles Based on Metal−Organic Framework DNA Biobarcodes Triggered G-Quadruplex Coupled with Rolling Circle Amplification Assay. *ACS Sens.* **2025**, *10*, 2136−2146.
(36) Bai, G.; Fan, Z.; Zhao, X.; Dong, Y.; Tan, C.; Bai, L.; Jiang, H.; Liu, T.; Li, J.; Zhao, X.; Yu, H. Highly Sensitive and Portable Detection of PD-L1^{+} Exosomes Using a Smartphone-Assisted Colorimetric Sensor. *Biosens. Bioelectron.* **2025**, *286*, No. 117592.
(37) Bain, C. D.; Troughton, E. B.; Tao, Y. T.; Evall, J.; Whitesides, G. M.; Nuzzo, R. G. Formation of Monolayer Films by the Spontaneous Assembly of Organic Thiols from Solution onto Gold. *J. Am. Chem. Soc.* **1989**, *111* (1), 321−335.
(38) Russo, M.; Teeuwen, R. W. H.; Flipse, C. F. J.; Albertazzi, L.; Zijlstra, P. Hot Charge Carriers Mediate Regioselective Thiol Cleavage and Biofunctionalization of Gold Nanoparticles. *ACS Appl. Mater. Interfaces* **2025**, *17* (49), 67295−67305.
(39) Maier, L.; Goemans, C. V.; Wirbel, J.; Kuhn, M.; Eberl, C.; Pruteanu, M.; Müller, P.; Garcia-Santamarina, S.; Cacace, E.; Zhang, B.; Gekeler, C.; Banerjee, T.; Anderson, E. E.; Milanese, A.; Löber, U.; Forslund, S. K.; Patil, K. R.; Zimmermann, M.; Stecher, B.; Zeller, G.; Bork, P.; Typas, A. Unravelling the Collateral Damage of Antibiotics on Gut Bacteria. *Nature* **2021**, *599* (7883), 120−124.
(40) Bertram, R.; Hillen, W. The Application of Tet Repressor in Prokaryotic Gene Regulation and Expression. *Microb. Biotechnol.* **2008**, *1* (1), 2−16.
(41) Yuan, Y.; Deng, J.; Cui, Q. Molecular Dynamics Simulations Establish the Molecular Basis for the Broad Allostery Hotspot Distributions in the Tetracycline Repressor. *J. Am. Chem. Soc.* **2022**, *144* (24), 10870−10887.
(42) Kaur, P.; Rana, S.; Singhal, S. Palladium-zinc Ferrite Varnished Hydroxyapatite Spherocuboids for Electrochemical Detection of Carcinogenic Food Preservatives. *Food Chem.* **2025**, *464*, No. 141626.
(43) Han, Y.; Wang, S.; Cao, Y.; Singh, G. P.; Loh, S. I.; Cheerlavancha, R.; Ang, M. C.; Khong, D. T.; Chua, P. W. L.; Ho, P.; Strano, M. S.; Marelli, B. Design of Biodegradable, Climate-Specific Packaging Materials That Sense Food Spoilage and Extend Shelf Life. *ACS Nano* **2023**, *17* (9), 8333−8344.
(44) Mpakanyane, T. E.; Nyokong, T. Electrocatalytic Sensing of Para-Hydroxybenzoic Acid Using Metalloporphyrin Microporous Polymers: Effect of the Central Metal. *J. Inorg. Organomet. Polym. Mater.* **2026**, *36*, No. 5147.
(45) Sun, S.; Song, P.; Sun, C.; Wang, J. A Novel Electrochemical Sensor Based on MOFs Composites, Gold Nanoparticles, and DNAzyme for Cu^{2+} Sensitive Detection. *J. Environ. Chem. Eng.* **2023**, *11* (1), No. 109151.
(46) Liu, M.; Zhu, H.; Wang, K.; Zhang, X.; Li, X.; Yu, M.; Zhu, B.; Sheng, W.; Liu, C. A Novel Fluorescent Chemodosimeter for Discriminative Detection of Cu^{2+} in Environmental, Food, and Biological Samples. *ACS Food Sci. Technol.* **2023**, *3* (1), 134−140.
(47) Li, H.-J.; Li, S.; Zhang, Y.; Liu, F.; Huang, Z.; Luo, J.; Zheng, F.; Yang, L.; Shi, K.; Han, F. Water-Induced Structural Instability in Zinc Coordination Polymers for Dual-Channel Fluorescent Sensing of Cu^{2+} and Cysteine. *Anal. Chem.* **2025**, *97* (25), 13422−13431.
(48) Liu, T.; Ramesh, A.; Ma, Z.; Ward, S. K.; Zhang, L.; George, G. N.; Talaat, A. M.; Sacchettini, J. C.; Giedroc, D. P. CsoR Is a Novel Mycobacterium Tuberculosis Copper-Sensing Transcriptional Regulator. *Nat. Chem. Biol.* **2007**, *3* (1), 60−68.
(49) Zhai, S.; Bai, M.; Yue, F.; Wang, H.; Huang, J.; Dong, H.; Yuan, B.; Li, Z.; Zhang, P.; Zhao, M.; Guo, Y.; Sun, X.; Zhao, W. Strip Biosensors Based on Broad-Spectrum Aptamers and Cationic Polymers for the on-Site Rapid Detection of Tetracycline Antibiotics Residues in Milk. *Food Chem.* **2025**, *464*, No. 141743.



https://doi.org/10.1021/acs.analchem.6c02971
Anal. Chem. XXXX, XXX, XXX−XXX